Chapter 10
Special Topics in Helium Cryogenics

In the preceding chapters, the emphasis has been on the properties of helium and its applications. However, there are numerous other topics in cryogenics which do not fall in this specific context but still have considerable relevance to the general subject of helium cryogenics. In the present chapter, three such topics are overviewed: (1) thermal insulation systems, (2) helium adsorption, and (3) magnetic refrigeration. The review of these subjects is not all-inclusive but rather represents a few areas of potential interest to the general subject of low-temperature phenomena important to the useful application of helium cryogenics.

10.1 Thermal Insulation

In the design of any cryogenic system, thermal isolation of the low-temperature environment must be achieved effectively. This is particularly true for low temperature helium systems owing to the small value of the latent heat of liquid helium and high cost per watt of refrigeration in this temperature range.

No thermal insulation system is perfect. The level of insulation can vary depending on the requirements of the application and the amount of effort applied. For very long life liquid storage tanks, the insulation is complicated and optimized to minimize the heat leak. Other systems that can tolerate a lower level of thermal isolation can have much simpler thermal insulation. However in any cryogenic application, the design and implementation of the thermal insulation system is a critical task.

There are various modes of heat transfer at play in a thermal insulation system. These involve different forms of the three principal modes of heat transfer:

1. Solid heat conduction through the structural supports, instrumentation wires and any insulating material.
2. Heat transport through any residual gas that may exist in the insulating vacuum space.

S.W. Van Sciver, *Helium Cryogenics*, International Cryogenics Monograph Series,
DOI 10.1007/978-1-4419-9979-5_10,

3. Radiant heat transfer from the surrounding to the low temperature environment.

Each of these modes is discussed below in the context of how it affects cryogenic insulation.

10.1.1 Solid Conduction

Solid conduction involves heat transport from high to low temperature through the materials of the insulating vessel. Some of these materials may be structural supports and others may be part of the insulation itself. This mode of heat transfer can be minimized by use of materials with low thermal conductivity and if necessary high strength. The relative importance of this mechanism depends on design. If the system demands a great deal of load transfer to ambient temperature, then the conduction heat leak will probably be an important contribution to the overall performance of the cryogenic system.

The conduction heat transfer can be calculated by application of Fourier's law for heat conduction,

$$\vec{q} = -k(T)\ \vec{\nabla}T \tag{10.1}$$

where *k(T)* represents the temperature dependent material thermal conductivity and $\vec{\nabla}T$ represents the temperature gradient in the direction of the heat flux, q. This property has been discussed for solid isotropic materials to a considerable extent in Chap. 2. For insulating materials, which are often anisotropic, the thermal conductivity will vary with direction as well as temperature.

Many practical problems involve one-dimensional conduction over a finite temperature difference. A commonly useful quantity in this case is the integrated or mean thermal conductivity, $\bar{k}$, which can be used for determining the total heat conduction between two fixed temperatures. The integrated thermal conductivity is defined by the expression

$$\bar{k} = \frac{1}{(T_2 - T_1)} \int_{T_1}^{T_2} k(T) dT \tag{10.2}$$

where T_2 and T_1 are the two end temperatures. In general, *k(T)* is a complex function of temperature making evaluation of (10.2) difficult. However, these thermal conductivity integrals have been tabulated for many materials of interest in cryogenics [1, 2].

For many materials at low temperatures, *k(T)* can be approximated over a limited temperature range by an expression of the form

$$k(T) = AT^n \tag{10.3}$$

Table 10.1 Integrated thermal conductivity in W/m K of several materials useful for low-temperature cryogenic storage applications [3]

Material	$\overline{k'}\Big\vert_1^4$	$\overline{k'}\Big\vert_4^{77}$	$\overline{k'}\Big\vert_{77}^{300}$
Stainless steel	0.2	4.5	12.3
G-10	0.04	0.27	0.66
Teflon	0.02	0.18	0.25
Nylon	0.005	0.13	0.28
Polystyrene	0.02	0.036	0.075
Styrofoam	0.009	0.011	0.023

where for metals in the helium temperature range $n \approx 1$ and for insulators $n \approx 3$. In that case, the integrated thermal conductivity (10.2) may be written

$$\bar{k} = \frac{A}{(n+1)} \left(\frac{T_2^{n+1} - T_1^{n+1}}{T_2 - T_1} \right) \tag{10.4}$$

Equation 10.4 indicates that as long as the thermal conductivity is a monotonically increasing function of temperature, $\bar{k}$ is dominated by the high-temperature end.

Table 10.1 gives some typical $\bar{k}$ values for materials that are common in low-temperature insulation systems. These are given for usual fixed boundary temperatures. To determine the conduction heat leak between temperatures other than those listed in Table 10.1, it is necessary to evaluate (10.2).

Some insulating foam materials have tabulated thermal conductivities that can be used for design of moderate performance cryogenic storage vessels, but normally not for the helium temperature range. The average thermal conductivity for two of these materials (polystyrene and Styrofoam) are also listed in Table 10.1. Normally, these foam materials have lower thermal conductivities than monolithic solids, with the possible exception of the very low temperature end. Note that the thermal conductivity of foam materials is a very complicated process because it involves solid conduction and conduction in the residual gas. Thus, the average thermal conductivity can vary depending on the application. For example, the thermal conductivity can increase by as much as 40% if air diffuses into the cells. This effect is even larger if light gases such as helium or hydrogen replace the air in the foam [4]. The thermal conductivity of foam can also be affected by moisture content [5]. Thus, the values for the foam insulations in Table 10.1 should be only used for approximate calculations.

10.1.2 Gas Conduction

The second important mode of heat transfer in a cryogenic storage container is conduction through the residual gas in the vacuum space surrounding the low-temperature environment. In principle, this mode can be made arbitrarily small by

reducing of the residual pressure to a very low value (typically $<10^{-3}$ Pa); however, such conditions are not always achievable. It is therefore important to be able to estimate the heat load due to a moderate vacuum condition.

To estimate the magnitude of the gas conduction heat leak, consider an ideal planer system consisting of two flat surfaces at different temperatures with a residual gas between them at pressure p. There are primarily two regimes of heat transport in the residual gas. The first represents the case where the mean free path l is short compared to the spacing between the two surfaces. Under this circumstance, the gas thermal conductivity and thus the heat leak is nearly independent of pressure except at low temperatures and high pressures (see Sect. 3.4). Gaseous conduction dominates the heat transfer for pressures in the range 1 Pa to 1 kPa. If the pressure is higher that this range free convection may further enhance the heat exchange with a process that is dependent on the geometry of the container, see Chap. 5. Such a situation would be catastrophic for a cryogenic storage vessel as it would result in a very high heat load.

For most applications pertaining to cryogenics, the residual pressure is considerably lower than this value. For lower pressures ($p < 0.1$ Pa) the heat transfer process is represented by a second regime, where the mean free path is greater than the distance between the two surfaces. The mean free path of a gas is discussed in detail in Chap. 3. This quantity is roughly equal to the inverse product of the number density, n, and the scattering cross section, σ,

$$l \approx \frac{1}{n\sigma} \sim \frac{k_B T}{\pi d^2 p} \tag{10.5}$$

assuming ideal gas behavior with k_B being Boltzmann's constant. For a residual pressure of 0.1 Pa, the mean free path for helium at 4.2 K is about 1 mm.

The regime where the mean free path is greater than the distance between the two surfaces can be evaluated in terms of molecular kinetic theory. The physical picture is that of molecules making several collision-free trips between the two surfaces before interacting with other molecules in the volume. Thus, the rate of heat transfer is more determined by the molecule-wall interaction than intermolecular behavior. In this regime, the heat transfer is approximately proportional to the absolute pressure. The molecule-wall energy exchange process is related to the extent to which the molecules come into thermal equilibrium with the wall. This process is measured in terms of an accommodation coefficient α given by [6]

$$\alpha = \frac{T_i - T_e}{T_i - T_w} \tag{10.6}$$

where T_i is the effective temperature of the incident molecule, T_e that of the emitted or reflected molecule, and T_w the wall temperature. The maximum value for α is of course unity, associated with the molecule coming into complete thermal equilibrium with the wall.

For parallel surfaces at temperatures T_1 and T_2, the heat flux by gas conduction at low pressures is given by the relationship

$$q = \frac{\alpha_0}{4}\frac{\gamma+1}{\gamma-1}\left(\frac{2R}{\pi MT}\right)^{1/2} p(T_1 - T_2) \tag{10.7}$$

Here γ is the ratio of the specific heats ($\gamma = 5/3$ for helium), and R is the universal gas constant in J/mol K, $T = (T_1 + T_2)/2$ is the average temperature and M is the molecular weight in kg/mole. The quantity α_0 is an averaged accommodation coefficient dependent on the individual accommodation coefficient and surface areas. For unequal values of α and A, the quantity α_0 must be averaged over the two surfaces, that is,

$$\alpha_0 = \frac{\alpha_1\alpha_2}{\alpha_2 + (A_2/A_1)(1-\alpha_2)\alpha_1} \tag{10.8}$$

The difficulty with applying this theory is that the value of α is known only approximately. For example, for very clean metallic surfaces near room temperature, the accommodation coefficient for helium gas is quite small because the molecules make nearly elastic collisions. A good approximate value for this regime is 0.025 [7]. At low temperatures, α increases approaching a value of about 0.6 at 20 K [8]. For many low-temperature applications, helium gas is the major contributor to gaseous conduction heat leak because most other gases condense or adsorb on the cold surfaces. For helium gas a reasonably good value to assume for average accommodation coefficients is around 0.5.

10.1.3 Radiation Heat Transfer

Thermal radiation represents the third mode of heat transfer which is of concern in cryogenic insulation systems. This mechanism is independent of residual gas pressure or structural supports. The usual method for reducing radiation heat leaks is to use one of various forms of multilayer shielding, a topic which is discussed later. In preparation for that discussion, the present section considers the basic aspects of radiant heat transfer at low temperatures.

The starting point for the description of thermal radiation heat transfer is to consider the spectral energy density associated with a black body, which is an idealized concept that assumes a body radiates the maximum energy flux as a function of wavelength. This energy flux is given by,

$$e_b(T,\lambda) = \frac{8\pi hc}{\lambda^5}\left(\frac{1}{e^{hc/\lambda k_B T} - 1}\right) \tag{10.9}$$

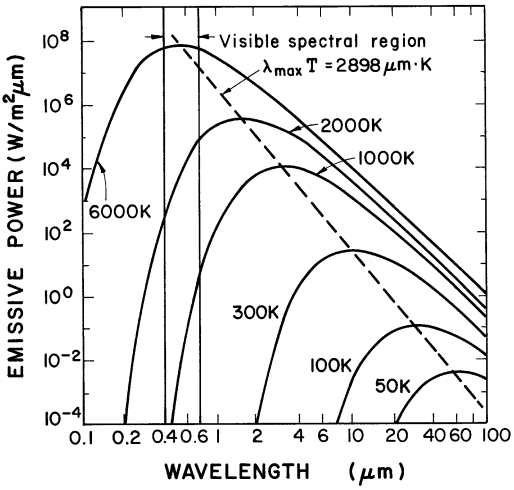

Fig. 10.1 Spectral energy density of black body radiation

where λ is the wavelength of the thermal radiation. This relationship has a well-known form shown in Fig. 10.1. At very high temperatures, the peak occurs in the range of visible spectrum, while at low temperatures the peak is shifted to longer wavelengths and has smaller amplitude. Wien's displacement law quantifies the temperature dependence of the peak wavelength:

$$\lambda_m T = 2898 \mu \text{m} \cdot \text{K} \tag{10.10}$$

Note that for surfaces at 4.2 K, the corresponding peak wavelength is 0.69 mm, which is in the far infrared. Such long wavelengths can have potentially important diffractive effects when the physical spacing between radiant surfaces approaches that of the peak wavelength [9].

For a black body the total radiant energy flux can be obtained by integration of (10.9) over all wavelengths. The integration produces what is known as the Stefan–Boltzmann law,

$$E_b = \int_0^\infty e_b(T, \lambda) d\lambda = \sigma T^4 \tag{10.11}$$

where σ is the Stefan–Boltzmann constant taking the value 5.67×10^{-8} W/m^2.

Most surfaces encountered in cryogenics do not approximate black bodies. In fact, the effort in cryogenics is usually one of minimization of the thermal radiation heat leak. If a surface is not black, its spectral energy density is smaller in proportion to its emissivity ε_λ. The emissivity is actually dependent on wavelength and is defined by the relationship

$$e_r(\lambda, T) = \varepsilon_\lambda e_b(\lambda, T) \tag{10.12}$$

where ε_λ is less than unity for nonblack surfaces.

It is often possible to make an approximation for radiant heat transfer which allows nonblack surfaces to be handled in a fairly straightforward manner. This assumption is to characterize surfaces as having constant emissivity less than unity, which is independent of wavelength. This is known as the *gray body* approximation and allows the writing of the total radiant energy flux as

$$E_r = \varepsilon \sigma T^4 \tag{10.13}$$

where the emissivity is determined for the appropriate set of conditions for the system of interest.

There are a number of implicit assumptions that enter into the *gray body* approximation. The first, already mentioned above, is that the emissivity must be wavelength independent over the range of wavelengths appropriate to the problem. Second, it is necessary to be able to equate the emissivity with the absorptivity a, which is a measure of the rate of energy absorption by the gray surface. The total absorptivity is defined by the relationship

$$E_a = aE_i \tag{10.14}$$

where E_i is the incident energy flux usually defined according to (10.13). Finally, for the gray body assumption to be reasonable, all surfaces must be diffuse scatterers of radiation. This is certainly far from the case for highly polished shields that often are present in cryogenic systems; however, it simplifies calculations considerably.

There have been numerous attempts to measure and tabulate the emissivities of different materials at low temperatures [10, 11]. Generally, these values are determined for radiant energy flux between ambient (273 or 300 K), liquid nitrogen (77 K), and liquid helium temperatures (4.2 K). A compiled graphical representation of emissivity measurements is shown in Fig. 10.2 [11]. To achieve low values of emissivity, it is necessary to have highly polished, high-conductivity surfaces made from gold, silver, copper, or aluminum. It has also been indicated [7] that since the emissivity is related to surface conductivity, it is best to polish the surfaces with a strain-free technique such as chemical etches. Finally, to estimate the radiant energy flux between surfaces of unknown emissivity, it is necessary to choose an approximate average value for ε. If the surface in question is dielectric, it is reasonable to assume black body heat transfer. If, on the other hand, the surface is a metal and polished, a conservative choice is $\varepsilon \approx 0.1$. However, as can be seen in Fig. 10.2, to achieve emissivities much less than 0.1, special care must be taken with the surface preparation.

The radiant heat transfer between parallel surfaces, shown schematically in Fig. 10.3, is a function of the properties of both surfaces. The rate at which energy is radiated from surface 1 is proportional to the emissivity ε_1, and the fourth power of the temperature T_1. A similar situation occurs for surface 2. In the simple case

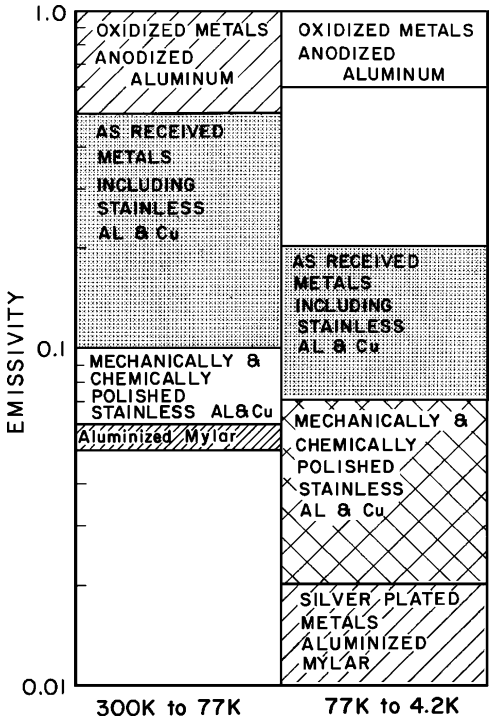

Fig. 10.2 The average emissivity of different metallic surfaces at fixed temperatures (Source: From Obert et al. [11])

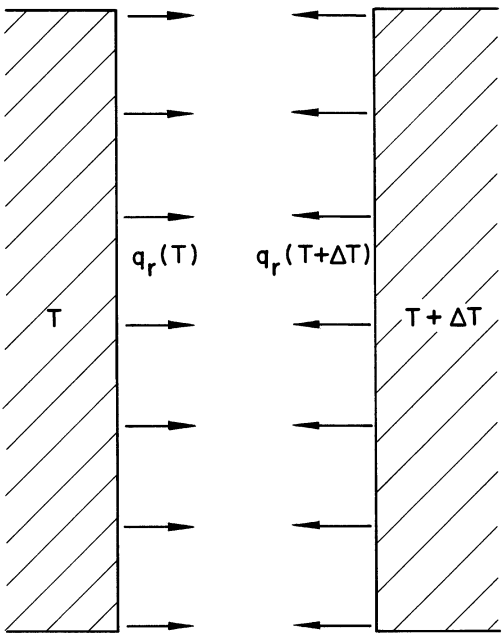

Fig. 10.3 Schematic of the radiant heat transfer process between two surfaces at different temperatures

that the surfaces can be approximated as black bodies, that is, $\varepsilon_1 = \varepsilon_2 = 1$, the net radiant heat flux is the difference between these two values:

$$q_r = \sigma\left(T_1^4 - T_2^4\right) \tag{10.15}$$

In the general case where the emissivity is considerably less than unity, the situation is more complicated. This is because the incident radiation from one surface can either be absorbed by the other or reflected back to the original surface. This problem can be solved by summing the infinite series of contributions to the radiant energy flux. The result for the net radiant heat flux for gray surfaces is

$$q_r = \left(\frac{\varepsilon_1 \varepsilon_2}{\varepsilon_1 + \varepsilon_2 - \varepsilon_1 \varepsilon_2}\right)\sigma\left(T_1^4 - T_2^4\right) \tag{10.16}$$

Note that in the special case often encountered in cryogenics where $\varepsilon_1 \simeq \varepsilon_2 \simeq \varepsilon \ll 1$, the quantity in brackets reduces to simply $\varepsilon/2$.

Example 10.1

Consider the heat leak to a vacuum insulated liquid helium container both with and without liquid nitrogen shielding. Assume that the residual vacuum is sufficiently low to be able to neglect gas conduction heat leak. Assume a fairly optimistic value for $\varepsilon = 0.05$ for both surfaces, and calculate the heat load/unit area.

Solution: Equation 10.16 yields a radiant heat leak between 77 and 4.2 K of $q_r(77\ \text{K}) \approx 50\ \text{mW/m}^2$, which for most systems is acceptable because it represents about 60 mL/h or liquid helium consumption per square meter of container surface area. If, on the other hand, the exterior surface is maintained at ambient temperature, 300 K, the heat leak is increased by approximately a factor of 300 which represents almost 3 L/h·m^2 of helium boil-off. Obviously, there is considerable benefit in liquid nitrogen shielding of liquid helium containers.

The above situation can be generalized to multiple radiation shields, which represents a fairly good approximation for aluminized mylar multilayer insulation (MLI) at low packing density, discussed below. For the case of n shields between two parallel surfaces, the radiant heat flux becomes

$$q_r = \left(\frac{\varepsilon_i \varepsilon_k}{(n-1)\varepsilon_i + 2\varepsilon_k}\right)\sigma\left(T_1^4 - T_2^4\right) \tag{10.17a}$$

where

$$\varepsilon_i \equiv \frac{\varepsilon_0 \varepsilon_s}{\varepsilon_s + \varepsilon_0 - \varepsilon_0 \varepsilon_s} \tag{10.17b}$$

and

$$\varepsilon_k = \frac{\varepsilon_s}{2 - \varepsilon_s} \tag{10.17c}$$

for which ε_0 is the emissivity of the two parallel surfaces and ε_s is that of the shields. For the special case where $\varepsilon_0 = \varepsilon_s = \varepsilon$, (10.17) can be simplified considerably:

$$q_r = \left(\frac{\varepsilon}{(n+1)(2-\varepsilon)}\right)\sigma\left(T_1^4 - T_2^4\right) \tag{10.18}$$

Note that for $\varepsilon \ll 1$, (10.18) predicts a heat leak reduced by the factor $(n + 1)^{-1}$ from that without the multilayer shields.

Example 10.2

Calculate the temperature of a thermally isolated radiation shield that is suspended between two fixed surfaces ($T_1 = 80$ K and $T_2 = 300$ K). Assume that all surfaces have a constant emissivity of 0.1.

Solution: If the shield is isolated then the only mode of heat transfer is by radiation. If we set the temperature of the shield as unknown, T_s, then the net radiant heat flux from the high temperature wall ($T_2 = 300$ K) to the shield must equal the net radiant flux from the shield to the low temperature wall ($T_1 = 80$ K),

$$q_r = \left(\frac{\varepsilon}{2}\right)\sigma\left(T_2^4 - T_s^4\right) = \left(\frac{\varepsilon}{2}\right)\sigma\left(T_s^4 - T_1^4\right)$$

Solving for T_s,

$$T_S = \left(\frac{T_1^4 + T_2^4}{2}\right)^{\frac{1}{4}} = 252.6 \text{ K}$$

It is an exercise for the student to show that the shield temperature is nearly independent of the T_1.

10.1.4 Multilayer Insulation (MLI)

Aluminized mylar with low-density fibrous insulating spacers between many layers, represents a special case of a multilayer insulation system. Since there is interlayer material present, it is no longer possible to assume that each of the n shields is isolated from the others except for the radiant heat transfer. This material is sometimes referred to as superinsulation or simply MLI (multi-layer insulation).

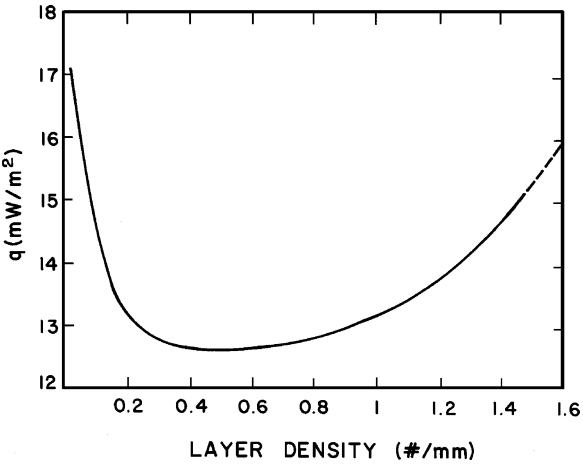

Fig. 10.4 Total heat exchange between two surfaces at 77 and 4.2 K as a function of layers of MLI (Source: Leung et al. [13])

Combined with high vacuum, MLI is the best insulating medium for low temperature systems and has become the standard for almost all cryogenic systems that operate in the liquid helium range.

With MLI there are two contributing heat transfer heat transfer mechanisms which are both functions of density and total number of shields. On the one hand, there is radiant heat transfer that decreases with increasing number of radiation shields, that is, layers of aluminized mylar. However, on the other hand, as the packing density increases, the heat transferred by conduction though the fibrous insulating spacers begins to make a larger contribution to the total heat leak. These two competing processes theoretically lead to an optimum layer density for practical multilayer insulations. Note that the solid-state conduction heat leak can be reduced by increasing the spacing between walls for the same packing density while the radiation contribution is only a function of number of layers. Therefore, the optimum number of layers should also be a function of the total insulation thickness or total number of layers.

The existence of a minimum in the layer density dependence of the heat transfer through MLI has been demonstrated experimentally [12, 13]. Plotted in Fig. 10.4 is one set of results for the heat flux through MLI between 4.2 and 77 K as a function of the numbers of layers [13]. The existence of a broad minimum near 0.5 layers/mm indicates the density where the solid-state conduction begins to play a substantial role. Note that the exact position of the minimum is not critical since a factor of two change in packing density increases the heat flux by less than 10%. Obviously, these results are not universal because the conduction and radiation contributions scale differently. However, MLI at low densities, less than 0.5 layers/mm, can be modeled fairly accurately by pure radiant heat transfer. For these results, the best choice for the emissivity of aluminized mylar is $\varepsilon = 0.011$ at 4.2 K and 0.03 at 77 K.

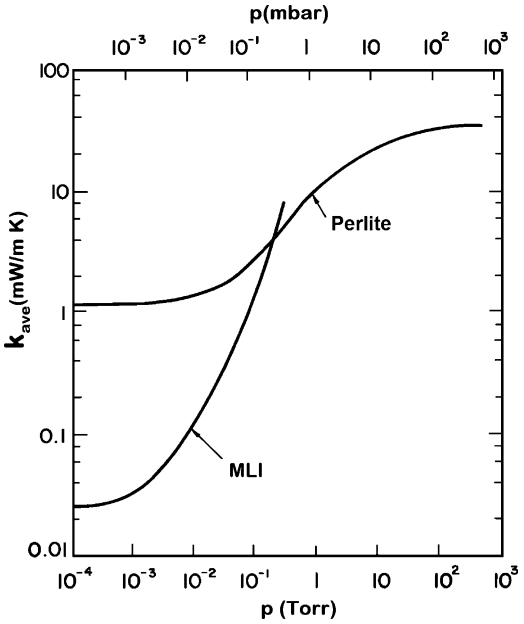

Fig. 10.5 Apparent mean thermal conductivity of glass powder and multilayer insulation versus residual gas pressure (Source: As compiled by Lady [15])

10.1.5 Powder Insulations

Glass powder insulation (the most common form is known as perlite) is also used to fill spaces between vacuum walls in insulating cryogenic vessels although it is not very common in helium systems [14]. This is because, in general, the performance of these materials is inferior to MLI. These materials generally are comprised of powders or glass microspheres with diameters in the range 10–1,000 μm. They have one clear advantage over MLI in that the material is easier to install, cheaper, and the residual vacuum requirements are not generally as stringent. However, the disadvantages of powder insulation technology are that it requires long and careful pump-down procedures and that the residual effective thermal conductivity is considerably greater than can be achieved with properly installed MLI at high vacuum. It is because of these latter two factors that powder insulations are most commonly used in large cryogenic storage tanks that contain the higher temperature cryogenic (LN_2, LNG).

The apparent thermal conductivity of perlite materials is a reasonably well-known quantity. Measurements have been carried out on the variation of this quantity with residual gas pressure. Most results are reported in the range of 77–300 K. Plotted in Fig. 10.5 are typical values for the apparent thermal conductivity of perlite versus residual gas pressure [15]. Note that minimum conductivity is achieved for pressures around 10^{-2} torr (~1 Pa) so lower pressures are not needed. For comparison, the figure also shows the apparent conductivity of superinsulation (MLI). In this case, a much

value is achievable at low pressures ($p \approx 10^{-4}$ torr or 10^{-2} Pa); however, at intermediate pressures, the benefits of superinsulation are minimal. At high pressures, $p \gtrsim 10$ Pa, superinsulation actually has higher thermal conductivity than the powders.

Recently, there has been a considerable effort at developing other porous insulations based on Aerogel, which is a very low density material containing a nano-pore structure. Some evidence suggests that these materials even in the intermediate pressure range have lower conductivities than perlite.

As a final comment, an additionally interesting problem concerns the refrigeration of radiation shields in cryogenic systems [16]. In large systems where radiation contributes substantially to the heat leak, it is possible to optimize the thermal performance by actively cooling the radiation shields. There are two main approaches to this problem. One approach, which is commonly used in cryostats that contain a stored cryogen (liquid helium storage vessels, for example) is to use the vented cryogen through tubes attached to the radiation shields. The vapor leaving the liquid container is nominally at the boiling point of the liquid and thus can intercept the radiant heat load at an intermediate temperature before venting from the cryostat.

An alternative approach that works with systems that are actively cooled is to again cool the radiation shields at intermediate temperatures but in this case with closed-cycle refrigerators. The advantage here is that improved overall thermodynamics can be achieved since radiation heat leaks from ambient temperature can be absorbed at higher temperatures, thus taking advantage of higher refrigeration efficiency. This approach often couples the conduction heat load to the intermediate cooling station for the same reasons. The thermodynamic principles needed to carry out this analysis are discussed in Chap. 8. For further details, the reader should consult references in the literature.

10.2 Helium Adsorption

Another interesting and technically significant topic related to the field of helium cryogenics is that of physical adsorption. Physical adsorption is a general term used to describe the process whereby an inert molecule comes in contact with and adheres to an inert surface or substrate. The inert character of each component is important because if substantial chemical reaction occurs, the process is referred to as chemisorption and the thermodynamics of the process are quite different. Since helium is inert and does not bond chemically to any other element, the adsorption process is described by physical mechanisms similar to those encountered in bulk condensation. It is often possible to treat the adsorbed film as an independent system, with the substrate forming the non-interactive boundaries much like walls of a container form the boundaries to bulk fluids.

Studies of adsorbed gases over the past few decades have expanded the understanding of the basic physical processes. Growth in the field can be attributed primarily to two factors. First, recent developments have introduced a number of experimental techniques for surface investigation. Several of these techniques are sensitive to less

than one atomic layer, allowing investigations of monolayer and submonolayer films. Second, scientists have discovered substrates that are regular and homogeneous and permit nearly ideal film behavior. Due to surface morphology, real surfaces tend to have considerable variability in adsorption potential which can result in inhomogeneous films. Although this situation is realistic in practice, it gives little insight into the detailed physical behavior of the film itself.

Physical adsorption has considerable technical importance in the field of cryogenics. One application is in cryopumping, a process whereby a gas is pumped from a system by exposing it to a large surface at low temperatures. This technology is used in numerous cryogenic devices and naturally occurs in liquid helium systems because the surfaces are so cold. When properly designed and used, cryopumps provide clean, oil-free vacuum systems with high capacities and essentially no moving parts. Another area of technical application for adsorption is in the separation of rarified gases. In this method, more strongly interacting molecules are adsorbed onto the substrate leaving the vapor phase enriched with the lighter more weakly bound molecules. Subsequently, the substrate can be "regenerated" by raising its temperature to desorb the heavier species. A major sector of the technology of air separation is based on this concept. Finally, adsorption is employed in a certain class of refrigerators that use the alternate condensation and evaporation of a fluid by adsorption/desorption as a process tool much like a compressor in a conventional cycle.

In addition to these technical uses, physically adsorbed layers can significantly impact the behavior of cryogenic processes and systems. For example, boiling surface heat transfer can be affected by the existence of adsorbed solid films which can interfere with the bubble nucleation process. Surface films can also impact the solid–liquid helium heat transfer process of Kapitza conductance by modifying the phonon transport. Radiative heat transfer can also be affected by variation of emissivity due to cryo-deposits on the surfaces. Finally, the adsorption of gas onto cold surfaces can represent a significant heat load to the system that can result in loss of stored cryogen. This topic was discussed in the context of the accommodation coefficient for molecular-kinetic heat exchange. All these factors make knowledge of the physical adsorption process important for proper understanding of the behavior of low-temperature systems.

10.2.1 Adsorption Thermodynamics

To begin, consider a simple thermodynamic description of the adsorption process. A closed container, shown in Fig. 10.6a, has N_v molecules in the vapor state at temperature T_v and an equilibrium pressure p. Assume that T_v is high enough that the molecules do not adhere in any significant numbers to the container walls, which are also at T_v. One of the container walls forms the adsorption substrate at a temperature T_s that can be independently regulated relative to T_v. Of interest are the physical processes that take place as the substrate temperature is reduced below T_v. Initially, as T_s decreases, the pressure will decrease also in rough proportion

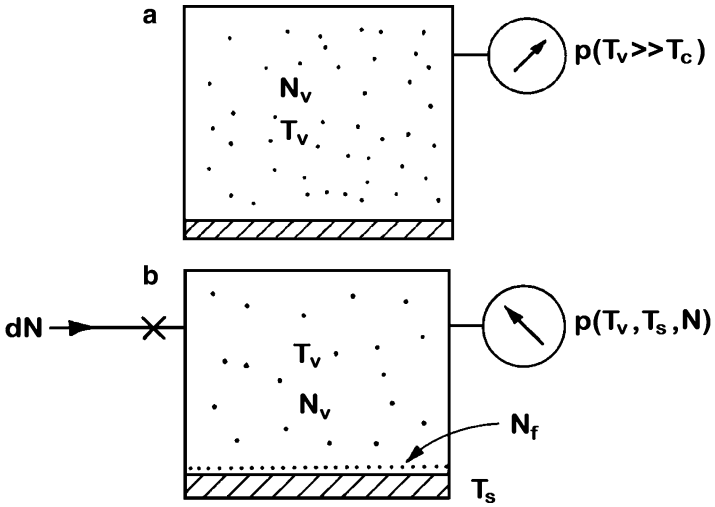

Fig. 10.6 Schematic representation of adsorption. (**a**) A closed volume with N_v, molecules in the vapor phase. The number of molecules adsorbed, N_f, is small compared to N_v because $T_s \gg T_c$. (**b**) The same volume with $T_s \lesssim T_c$ so appreciable adsorption occurs

because the vapor temperature will be some thermodynamic average of T_s and T_v. However, once T_s reaches a temperature of the order of the critical temperature of the vapor species, ~5 K in the case of ^{4}He, a substantial quantity of the gas will begin to adhere to the substrate.

The mechanism whereby this adherence occurs is the van der Waals interaction between the oscillating electric dipoles. A number of approximate potentials exist to model this interaction. One of these is the Lennard-Jones (LJ) 12-6 potential, which was introduced in Chap. 3 to describe interactions in real gases. In the case of an ideal two-dimensional planar surface comprised of substrate atoms, it is possible to write a modified form of the LJ potential for a gas atom a distance d above the plane [17],

$$U(d) = 4\pi\varepsilon n_s \left(\frac{\sigma^{12}}{45d^9} - \frac{\sigma^6}{6d^3} \right) \tag{10.19}$$

where n_s represents the density of substrate atoms and σ and ε are the Lennard-Jones parameters for the gas–substrate atom interaction.

Now consider the impact of introducing a small quantity of gas dN to the system. This situation is illustrated in Fig. 10.6b. If T_s is sufficiently low, some of the gas will be adsorbed, increasing the total particle number on the substrate by dN_f. The remainder will stay in the vapor such that $dN_v = dN - dN_f$. For a closed system in which this extra gas is introduced reversibly, the chemical potentials of each phase must be equal, $\mu_f = \mu_v$. This condition establishes a relationship between the entropy of each phase:

$$\left(\frac{\partial S_f}{\partial N_f} \right)_{E,A,V} = \left(\frac{\partial S_v}{\partial N_v} \right)_{E,A,V} \tag{10.20}$$

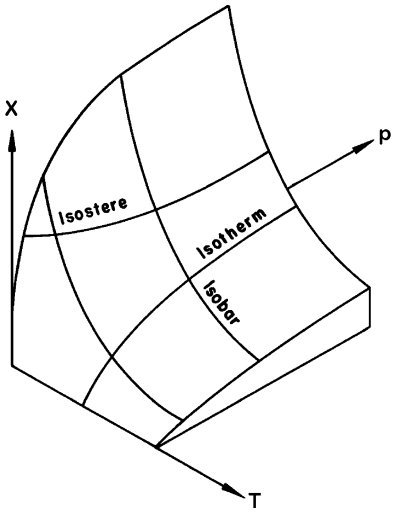

Fig. 10.7 An adsorption equilibrium surface. Lines of constant surface coverage are called isosteres

The behaviors of the two phases are related inherently through thermodynamics. For example, detailed information about the state of the film can be extracted from measurements of pressure of the equilibrium vapor phase.

In bulk matter, the behavior of the system is determined by an equation of state, a relationship between pressure, temperature, and volume. By analogy, in a film system an equation of state exists relating the three surface relevant parameters: spreading pressure φ, temperature T, and coverage or capacity x. However, under most conditions it is not possible to measure the film spreading pressure directly so that it must be inferred from bulk vapor pressure determinations. The most common situation is to construct an equation of state relating bulk vapor pressure, temperature, and capacity. Such a relationship is shown schematically in Fig. 10.7 which represents a surface equilibrium of an adsorption system. Note that processes occurring at constant capacity are referred to as "isosteric" by analogy with isochoric or constant volume processes in bulk systems.

One of the most important parameters in an adsorption system is the isosteric heat of adsorption, q_{st}. This quantity is defined as the amount of energy required to bring a molecule from the film into its equilibrium vapor. In the limit of zero coverage and at absolute zero, the isosteric heat is simply the single-particle binding energy to the substrate. As the film grows, this value decreases until for very thick films $q_{st} \rightarrow h_{fg}$, the heat of vaporization of a bulk condensate comprised of film molecules. These values form the limits for q_{st}. However, the detailed structure of this quantity can give considerable information about the thermodynamic state of the film.

The thermodynamic definition of q_{st} is given in terms of the entropy change at constant coverage:

$$q_{st} = -T\left(\frac{\partial S}{\partial N_f}\right)_{T,p,A} \tag{10.21}$$

By holding T, p, and A constant the variation of q_{st} is essentially along a constant coverage isostere; see Fig. 10.7. Substituting the relationship for equilibrium between the film and vapor, (10.20), we can rewrite (10.21) as a function of individual component entropies,

$$q_{st} = -T\left[\left(\frac{\partial S_f}{\partial N_f}\right)_{T,A} - \left(\frac{\partial S_v}{\partial N_v}\right)_{T,p}\right] \tag{10.22}$$

An alternate definition for the isosteric heat is given in terms of a temperature derivative of the equilibrium vapor pressure. This expression, which can be derived explicitly from (10.22) and is analogous to the Clausius-Clapeyron equation, is a function of easily measurable quantities:

$$q_{st} = k_B T^2 \left(\frac{\partial(\ln p)}{\partial T}\right)_{N_f,A} \tag{10.23}$$

In the simplest case where q_{st} is a constant, integration of (10.23) establishes an experimental form of the equilibrium vapor pressure,

$$\frac{p}{p_0} = e^{-q_{st}/k_B T} \tag{10.24}$$

where p_0 is a constant of integration. This expression identifies the importance that the isoteric heat plays in determining the ultimate pressure of an adsorption system.

The traditional method used for measurement of q_{st} is by vapor pressure isotherms. The behavior of the isotherms depends strongly on the type of substrate material and adsorbed gas. Substrate materials considered range from nearly ideal single-crystal surfaces to more practical inhomogeneous surfaces composed by polycrystalline metals or insulators. In addition, a given surface can be modified by first pre-plating the substrate with a more strongly adsorbed gas which then forms the new substrate for subsequent adsorption. Experimental data exist for numerous systems including almost all commonly available gaseous elements and a number of compounds. The temperature range of investigation in these studies is determined mostly by the strength of the gas–substrate interaction.

Most substrates encountered in practical adsorption problems are inhomogeneous, composed of polycrystalline or amorphous materials. Because of their non-uniformity, only qualitative models are available to describe their behavior. For inhomogeneous substrates the vapor pressure isotherm follows the general form shown in Fig. 10.8. Initially, the vapor pressure is quite low because the first layer is bound strongly. However, as the film builds thickness, the pressure increases rapidly until it asymptotically approaches that of the bulk liquid, p_s. An expression can be derived to compare with the results of Fig. 10.8 by assuming a layer-dependent form of q_{st} in (10.24). Considering only the attractive term in the van der Waals expression (10.19), we obtain the Frenkel–Halsey–Hill equation [17].

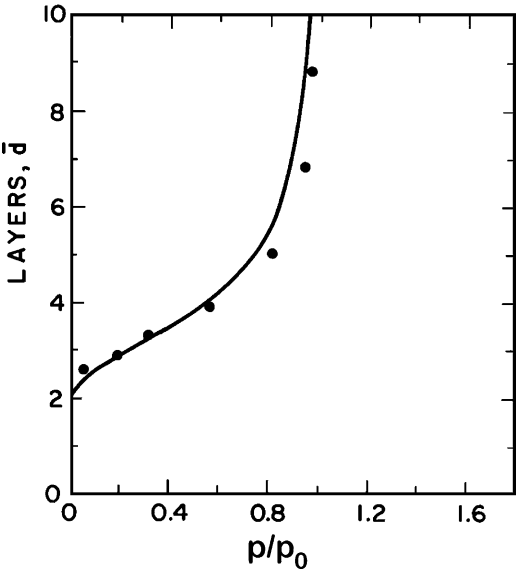

Fig. 10.8 An adsorption isotherm for a mylar substrate representing typical inhomogeneous character. The curve is based on the Frenkel–Halsey–Hill expression (10.25) (Source: Reprinted from Dash [17])

$$\frac{p}{p_s} = \exp\left(\frac{-\alpha}{k_B T \bar{d}^3}\right) \tag{10.25}$$

where α represents the strength of the attractive potential on the bare substrate and should be approximately equal to q_s, at low coverage, and d is the number of atomic layers. A comparison between the adsorption of ^{4}He on a mylar surface and that derived from (10.25) is made in Fig. 10.8. Theory and experiment are in qualitative agreement although the theory is not particularly sensitive to the detailed nature of q_{st}.

The limiting value of q_{st} is determined from the slope of low-coverage isotherms. One can also obtain information on the isosteric heat of adsorption by measuring the temperature dependence of the vapor pressure at constant coverage. For example, plotted in Fig. 10.9 is the absolute pressure versus T^{-1} for ^{4}He adsorbed on a copper sponge substrate. Note that the general form of (10.24) is obeyed. Furthermore, by extrapolation to zero coverage, it is possible to deduce an effective q_{st} for the substrate. These data yield a value $q_{st}/k_B \sim 160$ K. A number of different measurements of q_{st} for ^{4}He at low coverage are listed in Table 10.2. Note that the values of q_{st} for submonolayer ^{4}He are at least an order of magnitude larger than the latent heat of vaporization for helium, ~10 K. As a result, there can be a significant amount of adsorption of ^{4}He even at temperatures above T_c. However, the total quantities adsorbed are strong functions of temperature and are small because the process has an exponential dependence.

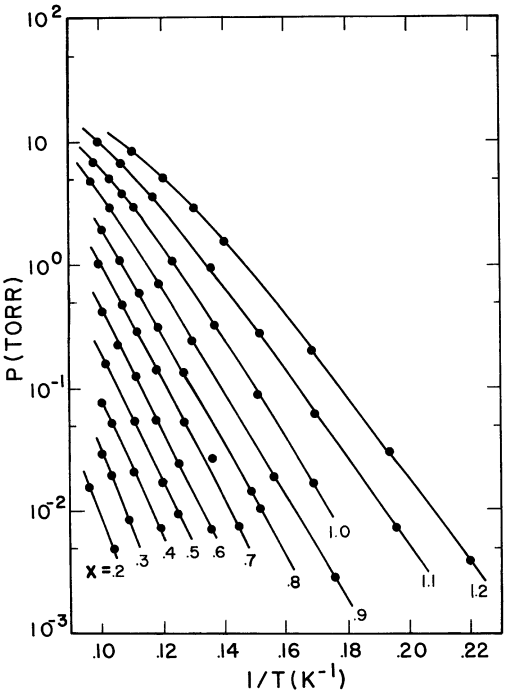

Fig. 10.9 Temperature dependence of the vapor pressure for constant coverage films on copper sponge. x refers to fractional monolayer coverage (Source: Reprinted from Princehouse [18])

Table 10.2 Isosteric heat of adsorption at low coverage for ^{4}He on various substrates

Substrate	q_{st}/k_B (K)	References
Copper	160	[18, 19]
Argon plated TiO_2	230	[20]
Exfoliated graphite	143–156	[21, 22]
Zeolite (13X)	220	[24]

As more gas is adsorbed on the surface the vapor pressure increases quite strongly. This effect can be seen most clearly in Fig. 10.8. Initially, the equilibrium vapor pressure is quite low due to the large value of q_{st}. However, as N_f increases, q_{st} decreases until for films having an equivalent thickness of four to six atomic layers the vapor pressure is essentially that of the bulk liquid or solid. The quantity of adsorbed gas necessary to complete one monolayer is an important parameter. Not only is this parameter an effective method of determining the surface area of the substrate but it also can be used as a fiducial point for estimating the density of submonolayer films. A number of methods exist for measuring monolayer completion. The most direct is to measure the vapor pressure isotherm. Above layer completion, the average position of the next absorbed gas molecule must be further from the substrate, and thus the molecule experiences a weaker binding. In an ideal

Table 10.3 ^{4}He capacities of various adsorbent materials

Substrate	Monolayer capacity (STP-cm^3/m^2)	Area (m^2/g)	References
Sintered Cu sponge (~μm^3 particles)	0.24	0.41	[18]
Zeolite 13X	0.29	527	[19, 23]
Exfoliated graphite	0.36	25	[22, 24]
Vycor glass	0.41	130	[25]

system the value of q_{st} would decrease discontinuously. However, most substrates are inhomogeneous and the layers are compressible so that, more commonly, q_{st} undergoes a change in slope at layer completion. The precise value of layer completion is also quite temperature dependent, owing to thermal excitations in the film, and therefore is defined only approximately for any substrate.

Listed in Table 10.3 are measured values for monolayer capacities of different substrates. Note that the capacity per unit area of substrate does not vary greatly from substrate to substrate. This is because the surface area is determined primarily by the hard sphere radius of the adsorbed molecule. On the other hand, there are wide variations of effective surface areas per gram of substrate material. Considerable benefit for cryopumping can be obtained by use of one of the high-surface-area materials. It should be pointed out that high adsorption capacity does not necessarily imply good cryopumping characteristics because the latter is a rate-dependent process. The rate at which adsorption occurs in high-surface-area materials is mostly a function of gas flow hydrodynamics within the material, a characteristic not necessarily desirable for high-speed cryopumps.

Vapor pressure isotherms are most commonly of the type described above, having a smoothly varying relationship between N_f and p. However, for some substrates that are very uniform this dependence is not observed. In these systems a discontinuous slope change in the vapor pressure isotherm occurs at monolayer completion. Further adsorption occurs on the second layer with a correspondingly lower value of q_{st}. This process continues until layer completion where a second step in the isotherm occurs. In the ideal case this mechanism for layer growth would continue indefinitely until the thermal excitations of the molecule of the order of k_BT blur the distinction between individual layers.

10.2.2 Physical Properties of Helium Films

Through the introduction of large-surface-area uniform substrates, it has become possible to investigate a number of interesting quasi-two-dimensional phases occurring mostly in the first one or two layers. The models that describe the physical processes emphasize the two-dimensional nature of the system. At low densities, much less than one atomic layer, helium adsorbed on graphite behaves much as a two-dimensional quantum gas. At high temperatures, its specific heat

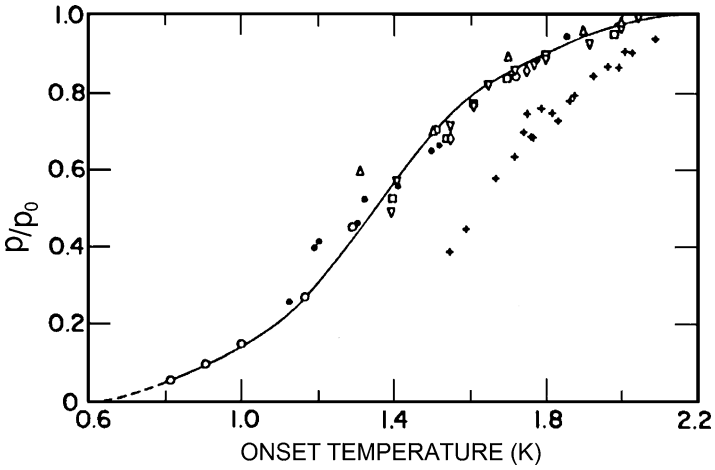

Fig. 10.10 Superfluid onset temperatures of ^{4}He films on different substrates and measured by different techniques (Source: From Herb and Dash [26])

asymptotically approaches a constant value of $C \approx Nk_B$, while at lower temperatures, quantum effects brought on by statistical correlations reduce the specific heat in a manner similar to the bulk fluids. At intermediate surface coverages, behavior occurs which can be correlated with regularity in the adsorbed gas. This effect is brought on by the adsorbed gas being affected by the periodicity of the substrate. At still higher coverages up to layer completion, the adsorbed gas sometimes behaves much as a two-dimensional solid with low-temperature specific heat varying as T^2, consistent with a two-dimensional Debye model. For these high coverages, melting transitions in the specific heat are observed at intermediate to high temperatures above which fluid-like behavior occurs. An interesting artifact of surface phases in adsorption systems is the occurrence of two-dimensional solids even though bulk helium does not solidify unless considerable external pressure is applied. In this case, the adsorption interaction compresses the molecules on the substrate to densities similar to those that occur in the bulk solid. These high densities allow the formation of long range order and crystal structure.

Of interest in unsaturated ^{4}He films is the question of when does superfluidity manifest itself. Clearly as was discussed in Chap. 6, thick saturated films display superfluidity in the form of film mobility (Rollin Film) and heat transport. For the case of unsaturated helium films of more than a few atomic layers, superfluidity is observed both in the λ-transition in the specific heat [24] as well as the onset of mobility [26]. The latter case is displayed in Fig. 10.10, which is a plot of the onset of superfluidity as a function of pressure ratio. Note the depression of the onset temperature with reduced film thickness as measured by the vapor pressure.

As was stated early on in this section, gas separation, cryopumping and adsorption refrigeration are the main applications for physical adsorption in cryogenic systems. In the first case the desired characteristics of the adsorbent are light weight, small heat

capacity, and large surface area. Typical materials used are activated charcoal, silica gel, activated alumina, or molecular sieves. The specific area of these materials are in the range 300–1,200 m^2/g and bulk densities less than 1 g/cm^3. No particular concern is given to surface uniformity. Applications generally call for designing an adsorption "bed" which provides good adsorption characteristics yet still allows for bulk flow. This application depends strongly on details of design.

In terms of cryopumping applications of adsorption, the choice of substrate material and configuration is more dependent on specific application. If high-speed pumping is required, the surface must not restrict the flow of gas. Therefore, the most common design is to use a planar metallic surface. To achieve substantial total pumping capacity before regeneration, this type of surface is necessarily quite large, a fact that leads to problems with reducing the radiation heat leak to warm surrounding surfaces. A number of standard techniques are available for providing radiation shields that allow high flow rates of gas. If high pumping speed is not necessary, use can be made of numerous high-surface-area materials, called "getters," thermally well anchored to a low-temperature heat sink. Getters of this type often are sealed into closed helium dewars to maintain good vacuum quality over an extended period of time.

Example 10.3

Calculate the vapor pressure of a three layer helium film adsorbed on a copper substrate at 4.2 K. Use the Frenkel–Halsey–Hill equation and assume $q_{st}/k_B = 160$ K. Compare the result with Fig. 10.8. Now use the same expression to estimate the vapor pressure of a monolayer film.

It is only necessary to calculate the ratio of the pressures,

$$\frac{p}{p_0} = e^{-\left(\alpha/k_B T d^3\right)}$$

For three layers (d = 3), this expression yields $p/p_0 = 0.24$, which is close to the value in Fig. 10.8. Now for d = 1 film, one calculates $p/p_0 = 2.8 \times 10^{-17}$, which is a physically unrealistic value but still emphasizes the strength of the adsorption process.

10.3 Magnetic Refrigeration

The use of the spin entropy of a magnetic system for cooling was first suggested in 1925 by Debye and Giauque [27–29]. It was then implemented by a number of groups in the 1930s. Today, magnetic refrigeration has been developed into a well-established technique for a number of specialized applications. The present section reviews this topic. We begin with a description of the physics of magnetic materials that is relevant to low temperature cooling. This discussion should provide the necessary understanding of the relevant properties of this special class of low-temperature materials.

Emphasis is given to the properties of some representative materials that have or are being used in magnetic coolers. Finally, some discussion of the practical aspects of magnetic refrigeration is presented with comments on the state of the art. The treatment is intended to introduce the microscopic and macroscopic aspects of paramagnetic cooling systems. For details, the reader should consult one of several recent publications on the subject.

There are essentially two distinct classes of magnetic refrigerators. One type of refrigerator operates down to the mK temperature range and is based on the electron spin states of paramagnetic materials. This refrigerator type will be emphasized here. The other type of magnetic refrigerator uses the nuclear spins of metallic elements to achieve temperatures in the μK range and as a result is more an expertise of low temperature physics.

10.3.1 Paramagnetic Materials

The paramagnetic salts are most commonly used in magnetic refrigerators. These materials have a number of characteristics in common. They are comprised of multi-component ionic molecules, one ion of which is magnetic. The magnetic ion is sufficiently dilute within the material that at high temperature it approximates a free non-interacting spin system. The strength of interaction determines the ordering temperature, below which the materials usually become diamagnetic. The ordering temperature of most paramagnetic salts is in the range below 1 K.

The theory of paramagnetic spin systems is developed around the statistical behavior of free magnetic ion systems. Any free magnetic molecule has two types of magnetic moment associated with its electron orbital structure. The first, due to orbital motion of the electron, is given the quantum number L. The other, resulting from uncompensated electron spins, has a quantum number S. The total angular momentum number J is the resultant of these two individual magnetic moments. In general, atoms have nonzero values of L and S. However, certain ions, particularly magnetic Fe^{3+} and Cr^{3+} and Gd^{3+}, have effectively an inert-gas orbital structure, so that $L = 0$, but they have uncompensated electron spins, such that $J = S$.

There are m_i different quantum numbers associated with each spin state of the atom, where m_i can take on values from $-J$ to J. Therefore, within each atom there are $2J + 1$ individual energy levels. Without the application of an external magnetic field, these levels are degenerate meaning that there is no distinction or energy level difference between them. However, in an external field this degeneracy is lifted, shifting the energy levels by an amount given by,

$$\varepsilon_i = -g\mu_B\mu_0 H m_i \tag{10.26}$$

where μ_B is the Bohr magneton which is a ratio of fundamental constants, $\mu_B = eh/4\pi m_e = 0.927 \times 10^{-23}$ J/T with e/m_e being the charge-to-mass ratio of an electron. The magnetic field is that which is felt locally by the atom and can be substantially

different from the applied magnetic field from external sources. The quantity g in (10.26) is known as the Landé g factor [30]. For many paramagnetic coolants with $L = 0$, $g = 2$.

For a material like gadolinium sulfate with $g = 2, J = 7/2$, the eight individual energy levels within the magnetic system have a level separation, $\Delta\varepsilon = 2\mu_B\mu_o H$, directly proportional to the magnetic field. At absolute zero in an applied magnetic field, all ions will occupy the lowest energy level. However, at finite temperature, some of the ions will be excited into higher levels based on their statistical distribution. Equating that energy level difference to the thermal energy of the ions, $k_B T$, one can show the significance of thermal excitation to the population of different levels.

$$\frac{\mu_0 H}{T} \approx \frac{k_B}{2\mu_B} \sim 0.75\left[\frac{T}{K}\right] \tag{10.27}$$

This relationship more or less establishes the boundary between the two regimes of ordering in a magnetic ion subsystem. The low-field, high-temperature regime occurs when the ratio $\mu_0 H/T \ll 0.75\ T/K$. In this regime, the magnetic ions essentially are disordered with the level spacing being small compared to $k_B T$. Since this is a disordered state, it is of higher entropy. On the other end of the spectrum, the high-field, low-temperature regime, $\mu_0 H/T \gg 0.75\ T/K$, corresponds to the majority of the spins occupying the lowest energy level. This is a lower entropy state for the spins.

Since the magnetic ion system consists of indistinguishable particles, it is appropriate to describe the behavior using Boltzmann statistics. The starting point for statistical analysis is the definition of a partition function, Z. For a magnetic ion system, the assumption is made that the total partition function is a product of the internal nonmagnetic part and the magnetic contribution,

$$Z_{total} = Z_{\text{int}} Z_B \tag{10.28}$$

In a magnetic ion system Z_B essentially is due to the Zeeman effect, the magnetic splitting in an external field. It can be shown that the Zeeman contribution to the partition function is [28],

$$Z_B = \frac{\sinh\left(J + \frac{1}{2}\right)a}{\sinh(a/2)} \tag{10.29}$$

where the parameter $a = g\mu_B\mu_0 H/k_B T$ is a measure of the ordering.

The low-temperature thermal properties of a magnetic ion system are considerably different from other more ordinary materials. Although these systems possess phonon excitations, a more dominant mechanism contributing to their thermal behavior at low temperature is due to the crystal field splitting of the ionic energy levels within the lattice [30]. Recall (Chap. 2) that the phonon specific heat is

proportional to T^3 at low temperatures. On the other hand the crystal field splitting, also referred to as the Stark effect, is caused by the ionic electric fields establishing different energy levels analogous to those from the magnetic Zeeman effect. The level splitting is small, typically on the order of 10–100 mK, and consequently only becomes important at low temperatures.

To derive an expression that adequately describes the Stark effect, we begin by making some simplifying assumptions concerning the structure of the energy levels. Often, crystal field splitting has associated with it two levels separated by an energy δ, with each level having a degeneracy g_n that is not lifted by the crystal field. In this case, we can write the partition function associated with the internal system as,

$$Z_{\text{int}} = g_0 + g_1 e^{-\delta/k_B T} \tag{10.30}$$

where g_0 and g_1 are the degeneracies of the ground and first excited states. The product of the two contributions to the partition function can be used to calculate the thermodynamic properties of the magnetic ion system.

The total entropy of such a system of spins is therefore made up of two terms,

$$S = N_m k_B T \left(\frac{\partial \ln Z}{\partial T}\right)_H + N_m k_B \ln Z \tag{10.31}$$

where N_m is the number of magnetic ions. Equation 10.31 can be differentiated to yield the specific heat and other thermodynamic variables. For example, the internal energy of the magnetic ion system is a function of the total partition function,

$$E = N_m k_B T^2 \left(\frac{\partial \ln Z}{\partial T}\right)_H + \mu_0 HM \tag{10.32}$$

The specific heat capacity at constant magnetization is just the temperature derivative of the internal energy, $C_M = (\partial E/\partial T)_M$. It therefore follows from (10.32) that the constant magnetization heat capacity is

$$\frac{C_M}{N_m k_B} = \frac{1}{N_m k_B}\left(\frac{\partial E}{\partial T}\right)_M = \frac{\delta^2}{k_B^2 T^2}\frac{(g_0/g_1)e^{\delta/k_B T}}{\left[1 + (g_0/g_1)e^{\delta/k_B T}\right]^2} \tag{10.33}$$

This expression, known as the Schottky equation, is plotted in Fig. 10.11 for different ratios of g_0/g_1. Note that the maximum in the Schottky heat capacity is approximately $½Nk_B$, which is very large compared to the other solid-state contributions at low temperatures. Note that N_m is the number of magnetic ions, which is generally much less than N, the total particle number. Also, typically, $\delta/k_B \approx 100$ mK so that this term dominates the zero field heat capacity at lower temperatures, $T < 1$ K.

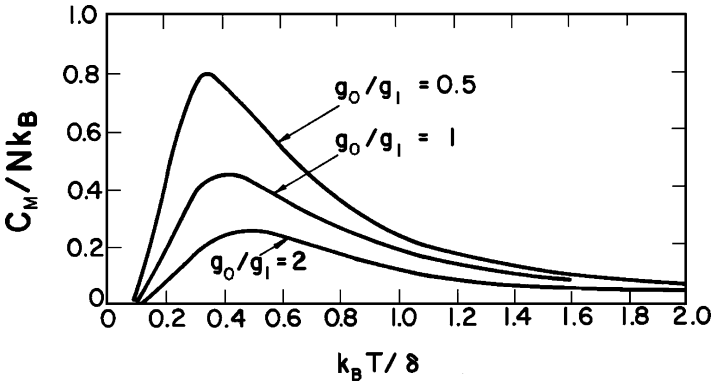

Fig. 10.11 Schottky heat capacity of a magnetic ion sub-system whose lowest energy level in the absence of any external magnetic fields is split into two states with degeneracies g_0 and g_1 (Source: From Zemansky [30])

For many magnetic refrigeration applications, the operating temperature is significantly above the Schottky anomaly temperature, δ/k_B. In this regime it is possible to take a high-temperature limiting form of (10.33) which yields

$$C_M = \frac{A}{T^2} \tag{10.34}$$

where A, the specific heat coefficient, has a value

$$A = N_m k_B \frac{g_0/g_1}{(1 + g_0/g_1)^2} \left(\frac{\delta}{k_B}\right)^2 \tag{10.35}$$

It is important to bear in mind that the above analysis applies to a system of N_m magnetic ions. Typically, in paramagnetic salts the magnetic ion number is much smaller than the total number of particles in the crystal. Therefore, if the heat capacity per unit mass or unit volume is desired, it is necessary to take into consideration the total molecular weight of the ionic salt.

The other important contribution to the specific heat of a magnetic ion system is that due to phonon excitations which at low temperatures, see Chap. 2. At low temperatures, this contribution may be approximated by the Debye model,

$$C_{\text{ph}} = 234 N k_B \left(\frac{T}{\Theta_D}\right)^3 \quad \text{for} T \ll \Theta_D \tag{10.36}$$

where N is the total atomic number and Θ_D is the Debye temperature typically >100 K.

We can compare the relative importance of the phonon and Schottky heat capacities based on the above discussion. Assuming for example that $g_0/g_1 = 0.5$ and taking the ratio of (10.34) to (10.36), we obtain

$$\frac{C_{\text{ph}}}{C_M} = 936\left(\frac{N}{N_m}\right)\left(\frac{T}{\Theta_D}\right)^3\left(\frac{k_B T}{\delta}\right)^2 \tag{10.37}$$

For a magnetic material like iron ammonium alum with $\delta/k_B = 242$ mK, $\Theta_D = 250$ K, and $N/N_m \simeq 50$, the above ratio at T = 1 K takes on the numerical value $C_{\text{ph}}/C_M = 0.052$. Therefore, the phonon contribution to the specific heat is already a minor (~5%) contributor at 1 K and becomes smaller as the temperature decreases, since the ratio goes as T^5. As a consequence, it is possible to neglect the phonon term for low temperature, T < 1 K applications. However, for many systems it must be included, particularly at high temperatures.

We now consider the magnetic properties of the paramagnetic materials. These are also given in terms of the magnetic partition function. For example, the magnetization can be obtained from a derivative of Z with respect to the applied magnetic field,

$$M = N_m k_B T\left(\frac{\partial \ln Z}{\partial \mu_0 H}\right) = N_m g \mu_B J B_J(a) \tag{10.38a}$$

where the quantity $B_J(a)$ is the Brillouin function,

$$B_J(a) = \frac{1}{J}\left[\left(J+\frac{1}{2}\right)\coth\left(J+\frac{1}{2}\right)a - \frac{1}{2}\coth\frac{1}{2}a\right] \tag{10.38b}$$

where as a reminder $a = g\mu_B\mu_0 H/k_B T$. In the limit of large a, there is a high degree of magnetic ordering and the magnetization approaches a constant value,

$$M = Ng\mu_B J \text{ for } g\mu_B\mu_0 H \gg k_B T \tag{10.39}$$

while at small values of a, the magnetic system is weakly ordered and the Brillouin function becomes linear with a. In this regime it is shown easily that the magnetization can be expressed as

$$M = \frac{\mu_0 \gamma_C H}{T} \text{ for } g\mu_B B \ll k_B T \tag{10.40a}$$

where γ_C is the Curie constant defined by expansion of the Brillouin function,

$$\gamma_C = \frac{N_m g^2 \mu_B^2 J(J+1)}{3k_B} \tag{10.40b}$$

Listed in Table 10.4 are specific heat coefficients for several paramagnetic materials along with other relevant properties.

Table 10.4 Selected properties of magnetic refrigerant materials[a]

Material	Specific volume (cm^3/g·ion)	Curie constant γ_C (J·K/g ion T^2)	Debye temperature Θ_D (K)	A (J K/g·ion)
$2Ce(NO_3)_3{\cdot}3M\ g\ (NO_3)_2{\cdot}24H_2O$	366	0–3.17[b]	60	5×10^{-5}
$Cr_2(SO_4)_3{\cdot}K_2SO_4{\cdot}24H_2O$	273	18.4	–	0.15
$Fe_2(SO_4)_3(NH_4)\ 2SO_4{\cdot}24H_2O$	282	43.8	250	0.108
$Gd_2(SO_4)_3{\cdot}8H_2O$	124	78	105	–
$Gd_3Ga_5O_{12}$	48	78	203	0.13

[a]See Refs. [29–33]
[b]Anisotropic material

10.3.2 Thermodynamics of Magnetic Refrigeration

The thermodynamic principles by which magnetic cooling can be achieved are seen easily by analogy with a fluid system. For the sake of simplicity, assume that the magnetic system is composed of a solid material so that pressure–volume work is negligible. In this case, the combination of the first and second laws of thermodynamics can be written

$$T\ dS = dE - \mu_0 H\ dM \tag{10.41}$$

where M is the magnetization of the material. Thus, the second term on the right-hand side is magnetic work done on the system by direct analogy to $p\ dV$, the work done in a fluid system.

Adiabatic demagnetization is analogous to isentropic expansion in a fluid system. The important parameter that controls this process is the isentropic coefficient, which for a magnetic system is the derivative of the temperature with respect to applied field at constant entropy:

$$\mu_m = \frac{1}{\mu_0}\left(\frac{\partial T}{\partial H}\right)_s \tag{10.42}$$

Note the similarity between (10.42) and the isentropic expansion coefficient defined in Chap. 8. Normally, μ_m is referred to as the magneto-caloric coefficient. Table 10.5 presents a comparison between parameters and coefficients relevant to magnetic and fluid refrigeration systems.

It is straightforward to show that μ_m is a function of the temperature dependence of the magnetization of the spin system,

$$\mu_m = -\frac{T}{C_H}\left(\frac{\partial M}{\partial T}\right)_H \tag{10.43}$$

Table 10.5 Comparison of parameters and coefficients in magnetic and fluid refrigeration systems

	Fluid	Magnetic
Extensive variable	V	M
Intensive variable	p	$\mu_0 H$
Work	$p\ dV$	$-\mu_0 H\ dM$
Isentropic coefficient	$\mu_s = \left(\frac{\partial T}{\partial p}\right)_s$	$\mu_s = \left(\frac{\partial T}{\partial H}\right)_s$

The application of (10.43) for a particular magnetic refrigeration system requires knowledge of two quantities, C_H and the temperature dependence of M. where the constant field heat capacity is

$$C_H = T\left(\frac{\partial S}{\partial T}\right)_H \tag{10.44}$$

Returning to the relationship for the magneto-caloric coefficient and considering a weakly interacting magnetic system obeying the Curie law, we find that μ_m takes on a simplified form,

$$\mu_m = \frac{M}{C_H} \tag{10.45}$$

which is analogous to the isentropic expansion coefficient for an ideal gas.

The other term needed to establish the behavior of a magnetic refrigeration system is C_H, the specific heat at constant magnetic field. A relationship for this quantity can be derived through application of the first and second laws of thermodynamics for a magnetic system (10.41). Defining the constant magnetization specific heat as

$$C_M = T\left(\frac{\partial S}{\partial T}\right)_M = \left(\frac{\partial E}{\partial T}\right)_M \tag{10.46}$$

then (10.41) can be recast into the form

$$T\ dS = C_M dT - \mu_0 H\ dM \tag{10.47}$$

Further restricting (10.47) to a constant magnetic field process, the expansion of the temperature differential defines the specific heat at constant field:

$$C_H = T\left(\frac{\partial S}{\partial T}\right)_H \tag{10.48}$$

It follows that C_H may be written

$$C_H = C_M - \mu_0 H \left(\frac{\partial M}{\partial T}\right)_H \tag{10.49}$$

As discussed above, the constant magnetization specific heat C_M is made up to several independent contributions. The relative importance of each contribution depends on the type of magnetic material involved and the temperature range over which cooling is to be achieved. Neglecting the phonon term, we obtain a simplified expression for the magneto-caloric coefficient:

$$\mu_m = \frac{\mu_0 \gamma_C H T}{A + \gamma_C \mu_0^2 H^2} \tag{10.50}$$

Subject to the above set of assumptions, this expression can be employed to determine the final temperature achieved by adiabatic demagnetization of a magnetic material. Here we simply integrate (10.50) over a finite change in field and temperature,

$$\int_{T_i}^{T_f} \frac{dT}{T} = \int_{\mu_0 H_i}^{\mu_0 H_f} \frac{\mu_0 \gamma_C H T}{A + \gamma_C \mu_0^2 H^2} d(\mu_0 H) \tag{10.51}$$

which by demagnetization to zero applied field, $H_f = 0$, results in the expression

$$\frac{T_i}{T_f} = \left(1 + \frac{\gamma_C \mu_0^2 H_i^2}{A}\right)^{1/2} \tag{10.52}$$

Example 10.4

Calculate the final temperature due to demagnetization of iron ammonium alum from 0.1 T initially at 1 K.

Inserting the appropriate values from Table 10.4: $A = 0.108$ J · K/mol and $\gamma_C = 43.8$ J ·K/mol into (10.52), the ratio of temperatures for $\mu_0 H_i = 0.1$ T becomes $T_i/T_f = 2.25$. Therefore, with the material initially at 1 K the final temperature as a result of adiabatic demagnetization would be $T_f = 0.45$ K. In practice, demagnetizing fields much larger than 0.1 T allow lower final temperatures, but the simplified expression derived above does not apply in that case since we have used the low field approximate solution.

Another way of approaching this problem is to consider the entropy in magnetic ion systems. In the limit of small magnetic field, $g\mu_B \mu_0 H \ll k_B T$ and for $T \gg \delta/k_B$ the spin entropy can be shown to obey the relationship [30]

$$S = N_m k_B \left(\ln(2J+1) - \frac{2(A + \mu_0 \gamma_C H^2)}{RT^2}\right) \tag{10.53}$$

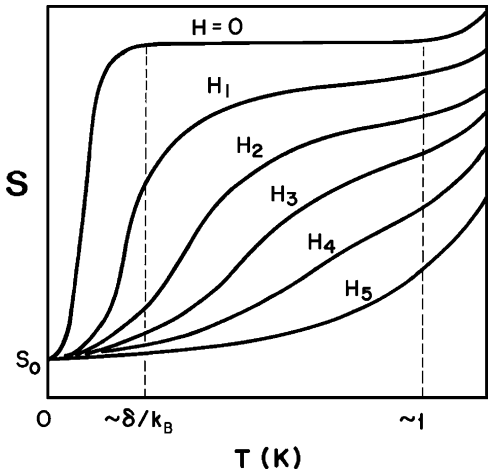

Fig. 10.12 Temperature–entropy diagram for a magnetic material

where J is the total angular momentum quantum number. Generally, except at very low temperatures ($T \ll 1\ K$), the first term in (10.53) is the dominant contribution to the spin entropy. This situation is desirable for magnetic cooling because the entropy change between the magnetized and demagnetized materials is what produces the cooling.

In the high magnetic field limit, $g\mu_B\mu_0 H \gg k_B T$, a considerably different situation occurs. Here the magnetic moments of the dipoles approach complete alignment with the magnetic field. The magnetic field is imposing a greater degree of order on the system, thus lowering the entropy. In the extreme case the spin entropy approaches zero, leaving the only remaining term associated with the Stark effect and the lattice, the latter of which can be neglected at low temperatures. In this limit, the principal behavior of the entropy is obtained by integration of the heat capacity (10.33). This analysis leads to an exponentially decaying entropy for the limit where $\delta/k_B \gg T$,

$$S = N_m k_B \left(1 + \frac{\delta}{k_B T}\right) \frac{g_0}{g_1} e^{-\delta/k_B T} \tag{10.54}$$

As the exact calculation of the entropy in a magnetic ion subsystem is dependent on choice of materials and operating range, it will not be carried out here. However, in order to calculate the final temperature of an adiabatic demagnetization, one needs to equate (10.53) with (10.54) and solve for the final temperature. This is a tedious, but straightforward calculation.

A schematic representation of the entropy of a magnetic ion subsystem is shown in Fig. 10.12. At high temperatures, $T \gg \delta/k_B$ and $T \gg g\mu_B\mu_0 H/k_B$, the entropy difference between the magnetized and unmagnetized state decreases because the

magnetic field is not very effective at magnetizing the sample. On the other hand, at very low temperatures, $T \ll \delta/k_B$ and $T \gg g\mu_B\mu_0 H/k_B$, the entropy difference decreases because the crystal field orders the system independent of the applied magnetic field. There is a range, indicated by the dashed lines in Fig. 10.12, over which the entropy difference $\Delta S \sim Nk_B \ln(2J+1)$, thereby allowing for efficient magnetic cooling. Obviously, the exact temperature range over which this region occurs depends on the particular paramagnetic material in question.

10.3.3 Continuous Magnetic Refrigerators

With the above survey of the thermodynamics of magnetic cooling, we now turn to the practical problems associated with achieving continuous refrigeration with magnetic materials. In this discussion emphasis is placed on continuous refrigeration rather than single-cycle adiabatic demagnetization, which was outlined above. The material that goes into a magnetic refrigerator must have a number of unique characteristics which set it apart from materials for other applications. Some of these characteristics have been introduced above, but a complete summary includes the following:

1. Magnetic refrigeration materials should have a small electronic and lattice specific heat. The energy used to cool the electrons and lattice is wasted and only reduces the efficiency of the cycle.
2. The magnetic level splitting due to the crystal field Stark effect, δ/k_B, should be below the range of operating temperatures. Otherwise, the entropy change with magnetization is reduced.
3. The magnetic contribution to the entropy should be large to allow more thermal energy to be cycled through the demagnetization process.
4. To achieve good thermal exchange with the systems to be refrigerated, it is desirable that the magnetic material have good heat transfer characteristics. Whenever possible, magnetic refrigeration materials should have a high thermal diffusivity.
5. Any material to be used in a device must be able to be fabricated into the configurations necessary for effective operation.

The principles of idealized closed-cycle magnetic refrigeration are similar to those for systems using fluids as working media. The most thermodynamically efficient cycle is the Carnot cycle which is a combination of isothermal and isentropic processes. This cycle can be achieved in a magnetic ion subsystem by a method shown schematically in Fig. 10.13, which is an actual T-S diagram for gadolinium sulfate. In this example, the Carnot cycle is shown as operating between two isothermal reservoirs at 15 and 1.7 K. This particular temperature range is attractive for magnetic refrigeration because helium gas–liquid cycles are limited to rather low thermodynamic efficiencies compared to the Carnot cycle. Also the maximum magnetization field of 10 T is a practical limitation because it allows

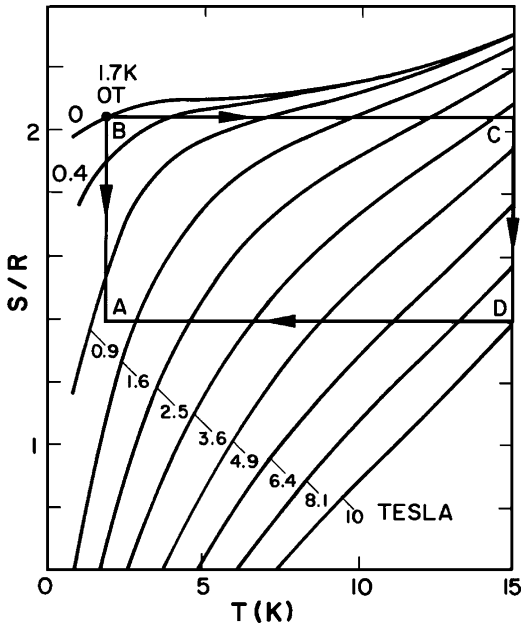

Fig. 10.13 Thermodynamic cycle executed by $Gd_2(SO_4)_3 \cdot 8H_2O$ in a magnetic Carnot cycle (from Steyert[30])

for the use of state-of-the-art but not prohibitively expensive superconducting magnet technology.

Consider the methods whereby Carnot refrigeration in a magnetic system can be achieved. A schematic diagram of the system is shown in Fig. 10.14. Apart from the reservoirs, the refrigerator consists of three principal components: the working material made of a magnetic salt, a magnet for aligning the spins of this material, and two thermal switches, one to either reservoir for exchange between the working material and isothermal baths. The Carnot cycle is a four-step process of magnetization, demagnetization, and heat exchange to the isothermal reservoirs.

The methods by which the Carnot cycle can be achieved are seen best by referring to the cycle ABCD in Fig. 10.13. With the thermal switch 1 (TS 1) closed and the working material in good contact with the heat reservoir (HR), the magnetic field is applied up to a maximum of 10 T represented by point D. Here the spins have the maximum alignment at this temperature.

Next, TS 1 is opened, isolating the magnetic material, and the field is decreased slowly, cooling the working material to point A at 1.7 K. Note that this point is not at zero field. Thermal switch 2 (TS 2) is then closed and the working material comes into the thermal equilibrium with the heat source. This step, which occurs isothermally, must be accompanied by a further slight demagnetization of the material to point B at which point all the heat has been transferred. Thermal switch 2 is then opened and the working material is magnetized slowly back to the high temperature represented by point C. Once the working material reaches the heat reservoir temperature, TS 1 is closed and further magnetization occurs isothermally to point D, completing the cycle. This process, as represented in Fig. 10.13, is able

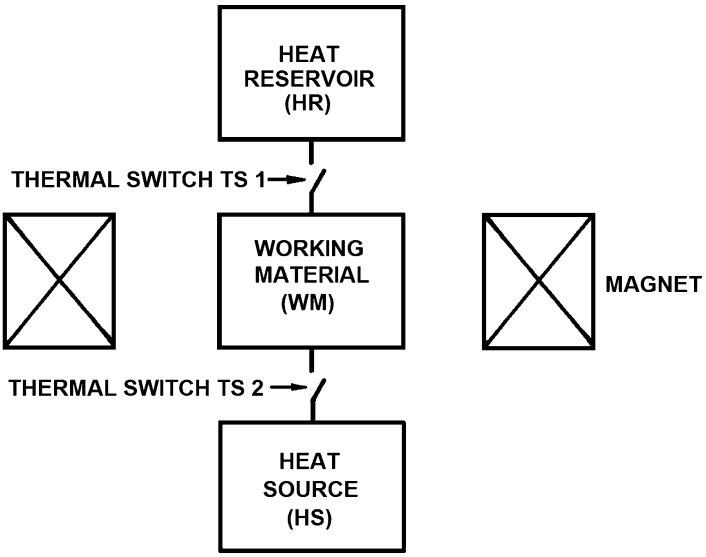

Fig. 10.14 Schematic diagram of magnetic Carnot refrigerator (Source: From Steyert [32])

to pump 27 J per liter of material per cycle, which if achievable at modest frequencies around 1 Hz could provide a rather high cooling rate in a very small volume. Of course, the difficulty in achieving this kind of cooling power lies in the practical aspects of creating a magnetic refrigerator.

In recent years there have been several devices built that are intended to bring the above concepts to realization on a practical scale [33–37]. In most cases the devices were developed to operate in the low-temperature region, $T < 4.2$ K, and to provide cooling power at the low end of the order of 1 W. Materials employed are either gadolinium sulfate or gadolinium gallium garnet (GGG), $Gd_3Ga_5O_{12}$. The latter material has shown superior thermal properties. In one particular case, a prototype refrigerator has been operated between 1.8 and 4.2 K with a cooling power of 1.2 W and an achieved figure of merit in the range of 45% [37].

10.3.4 Nuclear Demagnetization

To produce much lower temperatures with magnetic refrigeration it soon becomes inefficient to use paramagnetic salts as the working media because their spins will already be aligned. At these temperatures, which can span into the submillikelvin regime, it is possible to use the unpaired magnetic moment associated with the nuclei. The nuclear magnetic moment μ_N is smaller than the Bohr magneton by the ratio of nucleon to electron mass ($m_n/m_e = 1{,}840$). Thus, the nuclear spins can be aligned only by very high magnetic fields at low temperatures. This method was

first applied in 1956 by Simon and Kurti at Oxford where spin temperatures in the neighborhood of 10 μK were achieved through adiabatic demagnetization of the nuclei of a paramagnetic salt. However, the spin temperatures are not the same as the lattice temperatures and entropy must be transferred from one system to the other. The time constant that controls this process, called the spin–lattice relaxation time, can be large at very low temperatures, providing a severe hindrance to the ultimately achievable a microkelvin lattice temperature. In recent times, it has become more advantageous to achieve nuclear demagnetization using nuclei of metallic elements. In those systems the density of magnetic moments is much greater and the spin–lattice relaxation time shorter, allowing for minimum actual bulk temperatures. Record minimum bulk temperature of ~100 pK (10^{-10} K) have been achieved by multistage devices for which the last stage is nuclear demagnetization [38].

Questions

1. Explain why the apparent thermal conductivity of MLI has a minimum at a particular layer density. Sketch a graph of k_{app} vs. layer density. How would the graph be different if thickness of the MLI blanket were half as great, but the same number of layers used? Be as quantitative as possible.
2. If you wanted to improve heat exchange between two surfaces at low temperature, what would be the best gas to use? Why?

Problems

1. A 100 L spherical liquid helium Dewar consists of an inner vessel with a liquid nitrogen cooled shield surrounding the inner vessel. Both the helium vessel and nitrogen shield are suspended in a vacuum vessel. Assume that the emissivity of all surfaces is 0.1.

   (a) Calculate the heat load and liquid nitrogen consumption at 77 K.
   (b) Calculate the heat load at 4.2 K and liquid helium consumption.

   Neglect any contribution to the heat leak due to structural supports.
2. A liquid helium vessel (outer surface = 300 K) is surrounded by two, thermally insulated radiation shields. Assume that all surfaces have emissivities = 0.05. Calculate the temperature of the two shields and the heat leak per unit area to 4.2 K.
3. Calculate the pressure corresponding to a mean free path of 10 mm for a helium molecule at 80 K. Estimate the apparent thermal conductivity of helium gas under these conditions (Hint: you may assume that this is a free molecular flow condition). Let the spacing between walls be 10 mm.
4. Assume a monolayer of helium molecules forms a hexagonal closed packed structure. Use the hard core radius of a helium molecule to calculate the amount of gas at STP necessary to form one complete layer at low temperature. Compare your result with the data in Table 10.3.

References

1. Kittel, et al, Cryogenic Heat Transfer, Chapter 3 in *Handbook of Cryogenic Engineering*, ed. J. G. Weisend II, Taylor Francis, Philadelphia, 1998.
2. J. W. Ekin, *Experimental Techniques for Low Temperature Measurements*, Oxford University Press, 2006, pp. 514–5.
3. Values obtained from Cryocomp®.
4. R. F. Barron, *Cryogenic Systems*, 2nd Ed., Clarendon Press, Oxford, 1985.
5. J. E. Fesmire, et al, Cryogenic Moisture Uptake in Foam Insulation for Space Launch Vehicles, AIAA Conference Proceedings (2008).
6. E. H. Kennard, *Kinetic Theory of Gases*, McGraw–Hill, New York, 1938.
7. G. K. White, *Experimental Techniques in Low Temperature Physics*, 3 rd ed., Clarendon Press, Oxford, 1979.
8. R. J. Corrucini, Gaseous Heat Conduction at Low Pressures and Temperatures, *Vacuum* **7**–**8**, 19 (1959).
9. E. G. Cravalho, C. L. Tien, and R. P. Caren, Effect of Small Spacings on Radiative Transfer Between Two Dielectrics, *Transactions of ASME,* paper 67-HT-21 (1967).
10. P. F. Dickson and M. C. Jones, Infrared Spectral Reflectances of Metals at Low Temperatures, *Cryogenics* **8**, 24 (1968).
11. W. Obert, J. R. Coupland, D. P. Hammond, T. Cook, and K. Harwood, Emissivity Measurements of Metallic Surfaces Used in Cryogenics Applications, *Adv. Cryog. Eng.* **27**, 293 (1982).
12. K. D. Timmerhaus, Conductive Heat Transfer, in *Heat Transfer at Low Temperatures,* W. Frost (Ed.), Chap. 2, Plenum Press, New York, 1975.
13. E. M. Leung, R. W. Fast, H. L. Hart, and J. R. Heim, Techniques for Reducing Radiation Heat Transfer Between 77 K and 4.2 K, *Adv. Cryog. Eng.* **25**, 489 (1980).
14. R. H. Kropschot and R. W. Burgess, Perlite for Cryogenic Insulation, *Adv. Cryog. Eng.* **8**, 425 (1963).
15. E. R. Lady, Cryogenic Insulation, in *Cryogenic Engineering,* E. R. Lady (Ed.), Chap. 7, Engineering Summer Conference, University of Michigan, 1965.
16. Y. M. Eyssa and O. Okasha, Thermodynamic Systemization of Thermal Radiation Shields for a Cryogenic Apparatus, *Cryogenics* **18**, 305 (1978).
17. J. G. Dash, *Films on Solid Surfaces*, Academic Press, New York, 1975.
18. D. W. Princehouse, High-Resolution Heat Capacity Study of ^{4}He Adsorbed on Bare Copper, *J. Low Temp. Phys.* **8**, 287 (1972).
19. J. G. Daunt and E. Lerner, Adsorption of ^{3}He and ^{4}He on Various Substrates Below 30 K, *J. Low Temp. Phys.* **8**, 79 (1972).
20. W. A. Steele and J. G. Aston, Heats of Adsorption of Hydrogen and Helium on Prepared Surfaces, *J. Am. Chem. Soc.* **79**, 2393 (1957).
21. A. A. Antoniou, Adsorption of ^{4}He on Graphitized Carbon in the Submonolayer Region Between 2 and 15 K, *J. Chem. Phys.* **62**, 779 (1975).
22. R. L. Elgin and D. L. Goodstein, Thermodynamic Study of the ^{4}He Monolayer Adsorbed on Grafoil, Phys. Rev. **A 9**, 2657 (1974).
23. J. G. Daunt and C. Z. Rosen, Multilayer Adsorption of ^{3}He and ^{4}He on Zeolite from 4 to 80 K, *J. Low Temp. Phys.* **3**, 89 (1970).
24. M. Bretz, J. G. Dash, D. C. Hickernell, E. O. McLean, and O. E. Vilches, Phases of ^{3}He and ^{4}He Monolayer Films Adsorbed on Basel-Plane Oriented Graphite, *Phys. Rev. A* **8**, 1589 (1973).
25. D. F. Brewer, Some Thermal, Magnetic, and Flow Properties of Adsorbed He and He3-He4 Mixtures, *J. Low Temp. Phys.* **3**, 205 (1970).
26. J. A. Herb and J. G. Dash, Mass Transport of ^{4}He Films Adsorbed on Graphite, *Phys. Rev. Lett.* **29**, 846 (1972).

27. P. Debye, Einige Bemerkungen zur Magnetisieurung bei Taefer Temperature, *Ann. Phys*. **81**, 1154 (1926).
28. W. F. Giauque, Paramagnetism and the Third Law of Thermodynamics. Interpretation of the Low Temperature Specific Heat of Gadolinium Sulfate, *J. Am. Chem. Soc*. **49**, 1870 (1927).
29. W. F. Giauque and D. P. MacDogall, Attainment of Temperatures Below 1º Absolute by Demagnetization of $Gd_2(SO_4)_3 \cdot 8H_2O$, *Phys. Rev*. **43**, 768 (1933).
30. M. W. Zemansky, *Heat and Thermodynamics*, 5th ed., Chap. 14, McGraw–Hill. New York, 1968.
31. R. P. Hudson, *Principles and Application of Magnetic Cooling*, Chap. V, North Holland Publishing, Amsterdam, 1972.
32. W. A. Steyert, Magnetic Refrigeration, in *Liquid Cryogens*, Vol. 11, K. D. Williamson, Jr. and F. J. Edeskietz (Eds.), Chap. 6, CRC Press, Boca Raton, FL, 1983.
33. W. P. Pratt, S. S. Rosenblum, W. A Steyert, and J. A. Barclay, A Continuous Demagnetization Refrigerator Operating Near 2 K and a Study of Magnetic Refrigerants, *Cryogenics* **17**, 689 (1977).
34. R. Beranger, G. Bon Mardion, G. Claudet, C. Delpuech, A. F. Lacaze, and A. A. Lacaze, A Gadolinium Gallium Garnet Double Acting Reciprocating Magnetic Refrigerator, *Adv. Cryog. Eng*. **27**, 703 (1982).
35. A. F. Lacaze, A. A. Lacaze, R. Beranger, and G. Bon Mardion, Thermodynamic Aspects of a Double Acting Reciprocating Magnetic Refrigerator, *Proceedings of the 9th International Cryogenics Engineering Conference*, pp. 14–17, Butterworths, London, 1982.
36. A. F. Lacaze, R. Beranger, G. Bon Mardion, G. Claudet, and A. A. Lacaze, Double Acting Reciprocating Magnetic Refrigerator: Recent Improvements, *Adv. Cryog. Eng*. **29**, 573 (1984).
37. Y. Hakuraku and H. Ogata, A Rotary Magnetic Refrigerator for Superfluid Helium Production, *J. Appl. Phys.* Vol. 60, 3266 (1986).
38. J. T. Tuoriniemi and T. A. Knuuttila, Nuclear Cooling and Spin Properties of Rhodium down to Picokelvin Temperatures, Physica B, Volume 280, 474 (2000).

Further Readings

Cryogenic Insulation

R. F. Barron, *Cryogenic Systems*, 2nd Ed., Clarendon Press, Oxford, 1985.
E. H. Kennard, *Kinetic Theory of Gases*, McGraw–Hill, New York, 1938.
R. B. Scott, *Cryogenic Engineering*, Princeton Press, Princeton, NJ, 1959.
G. K. White, *Experimental Techniques in Low Temperature Physics*, 3 rd ed., Clarendon Press, Oxford, 1979.
F. P. Incropera and D. P. Dewitt, *Fundamentals of Heat Transfer*, Wiley, New York, 1981, Chapter 13.

Helium Adsorption

J. G. Dash, *Films on Solid Surfaces*, Academic Press, New York, 1975.
K. Wilson, Adsorption, in *Cryogenic Fundamentals*, G. G. Haselden (Ed.). Academic Press, London, 1971.
G. Davey, Cryosorption Pumping, in *Advanced Cryogenics*, C. A. Bailey (Ed.), Plenum Press, New York, 1971.

Magnetic Refrigeration

R. P. Hudson, *Principles and Application of Magnetic Cooling*, Chap. V, North Holland Publishing, Amsterdam, 1972.
G. K. White and P. J. Meeson, *Experimental Techniques in Low Temperature Physics*, 4 rd ed., Clarendon Press, Oxford, 2002.
M. W. Zemansky, *Heat and Thermodynamics*, 5th ed., Chap. 14, McGraw–Hill. New York, 1968.